

Definition of Distinct Compartments in Polarized Madin–Darby Canine Kidney (MDCK) Cells for Membrane-Volume Sorting, Polarized Sorting and Apical Recycling

Paul S. Brown^a, Exing Wang^a, Benjamin Aroeti^c, Steven J. Chapin^b, Keith E. Mostov^b and Kenneth W. Dunn^{a,*}

^a Department of Medicine, Indiana University School of Medicine, 1120 South Drive, FH115, Indianapolis, IN 46202-5116, USA

^b Department of Anatomy and Department of Biochemistry and Biophysics, University of California, San Francisco, CA 94143-0452, USA

^c Department of Cell and Animal Biology, The Hebrew University of Jerusalem, Givat Ram, Jerusalem, Israel

* Corresponding author: Kenneth W. Dunn, email: kdunn@iupui.edu

Previous studies of fibroblasts have demonstrated that recycling of endocytic receptors occurs through a default mechanism of membrane-volume sorting. Epithelial cells require an additional level of polar membrane sorting, but there are conflicting models of polar sorting, some suggesting that it occurs in early endosomes, others suggesting it occurs in a specialized apical recycling endosome (ARE). The relationship between endocytic sorting to the lysosomal, recycling and transcytotic pathways in polarized cells was addressed by characterizing the endocytic itineraries of LDL, transferrin (Tf) and IgA, respectively, in polarized Madin–Darby canine kidney (MDCK) cells. Quantitative analyses of 3-dimensional images of living and fixed polarized cells demonstrate that endocytic sorting occurs sequentially. Initially internalized into lateral sorting endosomes, Tf and IgA are jointly sorted from LDL into apical and medial recycling endosomes, in a manner consistent with default sorting of membrane from volume. While Tf is recycled to the basolateral membrane from recycling endosomes, IgA is sorted to the ARE prior to apical delivery. Quantifications of the efficiency of sorting of IgA from Tf between the recycling endosomes and the ARE match biochemical measurements of transepithelial protein transport, indicating that all polar sorting occurs in this step. Unlike fibroblasts, rab11 is not associated with Tf recycling compartments in either polarized or glass-grown MDCK cells, rather it is associated with the compartments to which IgA is directed after sorting from Tf. These results complicate a suggested homology between the ARE and the fibroblast perinuclear recycling compartment and provide a framework that justifies previous conflicting models of polarized sorting.

Key words: Endocytosis, endosome, epithelia, low density lipoprotein, MDCK, polarity, polymeric Ig receptor, transcytosis, transferrin

Received 9 August 1999, revised and accepted for publication 26 October 1999

The transport functions of an epithelium are determined by the distinct compositions of the apical and basolateral plasma membrane domains. This membrane polarity is maintained despite significant endocytic turnover, which in Madin–Darby canine kidney (MDCK) cells can amount to 40% of the plasma membrane internalized per hour (1). Whereas early studies indicated that the apical and basolateral endocytic recycling pathways of MDCK cells are distinct (2,3), recent evidence indicates that the two pathways are interconnected (4–6). With this continuous intermixing of apical and basolateral membranes, it is clear that endocytic sorting is crucial to maintaining the plasma membrane polarity of epithelial cells.

Some types of endocytic sorting are mediated by molecular signals contained in receptors. For example, endocytic sorting first occurs at the plasma membrane, in a signal-mediated interaction between receptor tails, clathrin and adaptor proteins (7). However, there is also ample evidence that default pathways exist in which proteins are sorted in the apparent absence of signals. Efficient recycling of endocytic receptors requires no specific signal, as the recycling of transferrin receptor (TfR) has been found to be unaffected by the deletion of the entire cytoplasmic tail (8). These studies, along with those of Mayor et al. (9), support a default model of receptor recycling in which membrane association alone is enough, in the absence of other signals, to guarantee efficient recycling (10). The high efficiency of this system is based upon the high surface-area-to-volume ratio of recycling vesicles, which enriches recycling vesicles with membrane proteins relative to lumenally-disposed ligands (11–13) and the repetition of this relatively low efficiency sorting step (10).

Recent studies, demonstrating similar concentrations of transmembrane proteins on sorting endosomes and recycling endosomes, indicate that default sorting may also operate in polarized MDCK cells (14). Unlike fibroblasts, however, polarized cells require an additional mechanism for polarized membrane sorting. Studies of MDCK cells (4) suggest that polar sorting occurs after membrane-volume sorting in a compartment downstream of the sorting endosome, termed the apical recycling endosome (ARE). This model is supported by recent studies indicating that polar sorting occurs downstream of sorting endosomes in an apical compartment enriched in rab11 (15), a protein previously associated with the ARE of both MDCK (16) and gastric parietal cells (17). Similar sub-apical compartments have been identified in a variety of epithelial cells (reviewed in (18)) and implicated in polarized sorting in Caco-2 intestinal cells (19), HepG2 hepatoma (20) and Eph4 mammary epithelial cells (21).

However, similarities between the ARE and the perinuclear recycling compartment (PRC) of certain fibroblasts suggest that even this membrane pathway may be common to both polarized and non-polarized cells (18). Like the PRC, the ARE is a pericentriolar terminal membrane recycling compartment, whose structure depends upon microtubules and is associated with rab11a and rab17 (4,16–18,20–22). These similarities raise the exciting possibility that the PRC, whose function is not understood, may be homologous to the ARE and may be a cognate polar sorting compartment in fibroblasts (4,21).

The role of the ARE in polar sorting is questioned by the studies of Barroso and Sztul (23), which indicate that TfR, a basolateral membrane protein, does not pass through the ARE of MDCK cells. An alternative model is that polarized sorting occurs on tubular extensions of sorting endosomes, as suggested by studies of rat liver cells (24). This model is supported by recent studies of glass-grown MDCK cells showing that apically-targeted IgA and basolaterally recycling transferrin (Tf) are enriched in separate populations of vesicles budding from tubular extensions of sorting endosomes (25). However, the efficiency of vesicular sorting was much lower than the overall efficiency of polarized sorting, leaving open the possibility that the majority of polar sorting occurs in the ARE, a question that could not be addressed as the incompletely polarized cells of this study lacked a discernible ARE.

Studies of the ARE are hindered by the fact that there are currently no methods for its isolation. We show here that the ARE of MDCK cells is readily distinguishable by multicolor confocal microscopy and can be characterized using quantitative image analysis. Taking advantage of this, we have used MDCK cell lines transfected with the rabbit pIgR (polymeric immunoglobulin receptor) and human TfR to address the role of the ARE in polarized sorting in polarized cells. Fluorescent conjugates of dimeric immunoglobulin A (IgA), Tf and low density lipoprotein (LDL) were used to vitally label the transcytotic, recycling and lysosomal pathways, respectively. Multicolor confocal microscopy of cells incubated with various combinations of these probes was used to functionally identify different types of endosomes on the basis of their ligand contents. Endocytic compartments were labeled by brief incubations comparable to the kinetics of endocytic sorting and quantitative microscopy of live and fixed cells was then used to identify the sites and quantify the efficiency of intracellular sorting in individual cells.

These studies distinguish two sequential steps of endocytic sorting in polarized MDCK cells and indicate that polar sorting occurs in recycling endosomes preceding the ARE. Quantitative microscopy demonstrates that, following internalization into lateral sorting endosomes, Tf and IgA are sorted from LDL, but not from one another, into recycling endosomes that distribute throughout the medial and apical regions of the cell. While Tf is directly recycled to the basolateral membrane from recycling endosomes, IgA is sorted to the ARE

prior to delivery to the apical plasma membrane. Although frequently lacking a condensed ARE, non-polarized MDCK cells likewise efficiently sort IgA to an intracellular compartment prior to efflux. IgA and Tf are non-selectively sorted from LDL in a manner consistent with the default process of membrane-volume sorting observed in fibroblasts. However, the absence of Tf traffic through the rab11-containing ARE complicates the putative homology between the ARE and the fibroblast PRC, which regulates the rate of Tf recycling in fibroblasts via rab11 (22,26). The distinction of two compartments in the apical cytoplasm of polarized MDCK cells, both of which satisfy the criteria previously used to identify the ARE, requires careful reconsideration of many previous studies of the function and regulation of the ARE, particularly with respect to polarized sorting.

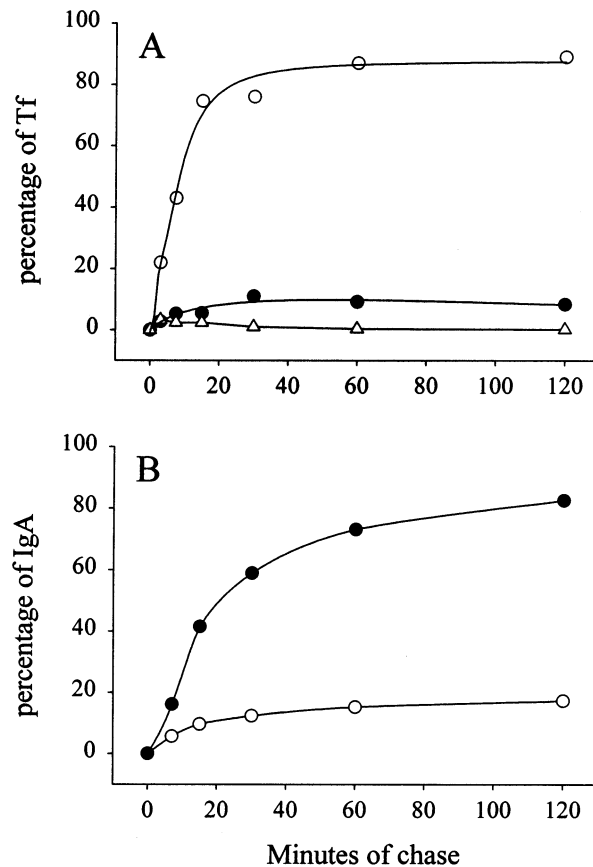


Figure 1: Kinetics of Tf and IgA recycling and transcytosis.

Approximately 80% of basolaterally internalized Tf is recycled to the basolateral medium, while ~80% of basolaterally internalized IgA is transcytosed to the apical medium. Polarized monolayers of PTR9 cells were incubated from the basolateral side with ^{125}I -Tf for 2 h at 18°C (A) or ^{125}I -IgA for 5 minutes at 37°C (B) and then washed and re-incubated in the absence of radio-labeled ligand at 37°C. The rates of label effluxed to the apical (closed circles) or to the basolateral (open circles) media and the amount of surface-bound Tf (triangles) were calculated as described in Materials and Methods.

Results

Polarity of the TfR and kinetics of Tf and IgA transport

In order to validate the transfected PTR9 cell system as a model of Tf and IgA endocytosis, the kinetics of ^{125}I -Tf and ^{125}I -IgA recycling and transcytosis were measured (see Materials and Methods). Figure 1A shows that basolaterally internalized Tf is efficiently recycled to the basolateral medium with a half-time of approximately 8 minutes, with minimal apical transcytosis. Figure 1B shows the kinetics of the basolateral-to-apical transcytosis of IgA, which occurs with a half-time of approximately 15 minutes. These kinetics agree well with previously published values for the parental cells (4) and for another MDCK cell line transfected with the human TfR (6).

Measurements of ^{125}I -Tf binding to the surface of polarized cells at 4°C show that 85% of the receptor is expressed basolaterally. These results are qualitatively supported by microscopic observations that showed minimal apical uptake of fluorescent Tf by polarized monolayers. The polarity and impermeability of the monolayers used for microscopic analyses were established by a variety of criteria (see Materials and Methods).

Tf, IgA and LDL internalize into the same sorting endosomes

In order to morphologically characterize the itineraries of Tf, LDL and IgA within polarized cells, polarized monolayers

were incubated with fluorescent ligand analogs for various periods of time and then fixed for examination by confocal microscopy. Within 2 minutes of addition of fluorescent ligands to the basolateral side of polarized monolayers of PTR9 cells, fluorescent endosomes begin to appear along the lateral membranes of the cells. Panel E of Figure 2 shows a stereopair representation of the distribution of F-Tf in filter-grown MDCK cells following a 2 minutes basolateral incubation at 37°C. Note that this and all following stereopairs are also represented as movies of rotated projections on the website located at <http://journals.munksgaard.dk/traffic/> videogallery

As has been previously demonstrated in other cell systems (24,27), different endocytic probes are internalized into the same sorting endosomes. Figure 2 shows examples of cells labeled basolaterally for 2 minutes at 37°C with both dil-LDL and F-Tf (panels A,B) or with both TxR-Tf and OG-IgA (panels C,D). The extensive colocalization of the pairs of endocytic ligands is apparent throughout the fields, but arrows can be used for orientation towards constellations of punctate sorting endosomes containing colocal probes. Note that the ratios between the two probes vary between endosomes, but colocalization is nearly complete.

The identity of these fluorescent accumulations as endosomes is confirmed by the lack of such structures in cells incubated for 60 minutes at 4°C in the presence of basolateral dil-LDL (panel F) or OG-Tf (panel G). The endosomal

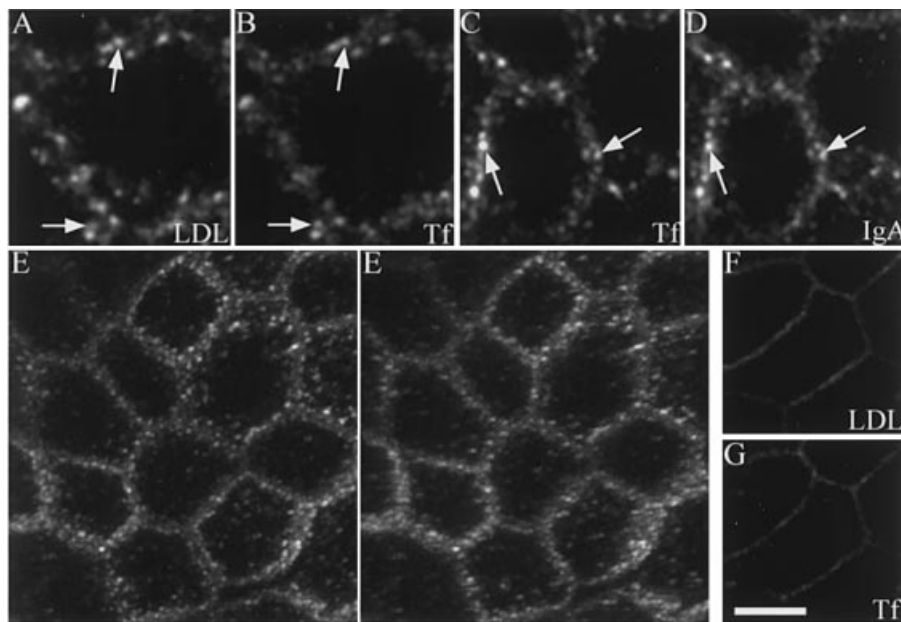


Figure 2: Tf, LDL and IgA are internalized into the same lateral sorting endosomes. Filter-grown PTR9 cells were incubated from the basolateral side for 2 minutes at 37°C with both dil-LDL and F-Tf (panels A and B, respectively) or with both TxR-Tf and OG-IgA (panels C and D, respectively) and images collected by confocal microscopy. Although the ratio of ligands varies between endosomes, extensive colocalization is seen between each pair of probes. Panel E shows a stereopair projection of a field of cells fixed after a 2 minutes basolateral incubation with F-Tf. In this and all following stereopair images, the apical side of the cells will appear towards the viewer when using a stereo-viewer, but will appear away from the viewer when viewed cross-eyed. Note that this and all following stereopairs are also represented as movies of rotated projections on the website located at <http://journals.munksgaard.dk/traffic/> videogallery Panels F and G show fields of cells incubated for 60 minutes at 4°C with dil-LDL and F-Tf, respectively. The length of the scale bar reflects 5 μm in panels A–D and 7 μm in panels E–G.

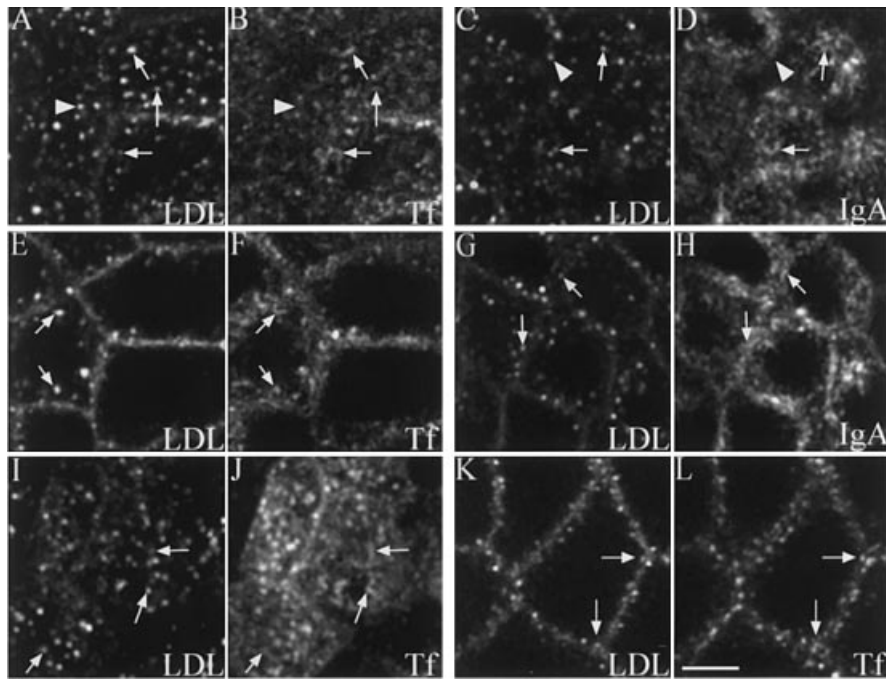


Figure 3: Tf and IgA are sorted from LDL to recycling endosomes. Within 10 minutes of continuous incubation, Tf and IgA are found in both vesicles that contain LDL, but also in recycling endosomes depleted of LDL and distributed throughout the cell. A supranuclear focal plane showing dil-LDL and F-Tf fluorescence of a field of cells incubated for 10 minutes is shown in panels A and B, respectively. A corresponding pair of images collected 3.5 μm lower, at the level of the nuclei is shown in panels E and F. A supranuclear focal plane showing dil-LDL and OG-IgA fluorescence of a field of cells incubated for 10 minutes is shown in panels C and D, respectively and a corresponding pair of images collected 1.8 μm lower, at the level of the nuclei is shown in panels G and H. Within 10 minutes LDL also starts to appear in late endosomes lacking Tf or IgA (arrowheads). Panels I and J show a field of live cells imaged in the presence of dil-LDL and OG-Tf, respectively. Panels K and L show a field of cells incubated for 10 minutes with dil-LDL and OG-Tf, respectively, after prior treatment for 60 minutes with 33 μM nocodazole. In each panel arrows indicate tubular Tf or IgA partially overlapping vesicular LDL. The scale bar is 10 μm in length.

nature of these lateral accumulations is also indicated by the fact that comparable structures seen in live cells are acidified (Wang et al., in preparation).

Tf and IgA are sorted from LDL into recycling endosomes

The subsequent stages in the endocytic itinerary of Tf, IgA and LDL were characterized by incubating cells basolaterally with fluorescent ligands for 10 minutes at 37°C. Significant changes in the distribution of each ligand occur during the interval between 2 and 10 minutes of continuous incubation. Tf, IgA and LDL redistribute both apically and towards the inner cytoplasm of each cell. Moreover, during this time a significant fraction of Tf or IgA is no longer coincident with the punctate compartments containing dil-LDL, but is now distributed in tubular recycling endosomes, many of which appear to be in continuity with the LDL-containing vesicles.

The relative distributions of the various ligands can be precisely assessed by comparing images of each probe in individual focal planes. Figure 3 shows images of cells incubated with LDL and Tf for 10 minutes, collected both above and at the level of the nuclei (Panels A,B and E,F, respectively). After 10 minutes of incubation, Tf is now found not only colocalized with LDL in vesicular structures, but also dis-

tributed in delicate, apparently tubular structures, some of which appear to be continuous with the vesicular compartments containing LDL (noted with arrows). Arrowheads indicate compartments containing LDL but no Tf, which are likely to be late endosomes. These observations are corroborated in observations of living cells that again display punctate LDL and tubular Tf distributions (Panels I and J, respectively).

Images of supranuclear and circumnuclear planes of cells labeled for 10 minutes with dil-LDL and OG-IgA are strikingly similar to those of cells incubated with fluorescent LDL and Tf. As with Tf, fluorescent IgA is found to strongly label tubules that frequently appear to be continuous with LDL-containing vesicles (noted with arrows) and are found throughout the cell, both above the nuclei (Figure 3, panels C,D) and in medial planes (panels G,H). Comparison of these figures also shows that, in contrast to recent studies (25), the formation of tubules does not depend on the presence of IgA, as Tf can be found in a tubular distribution in the absence of IgA. A similar extensive, delicate endosome morphology was found in a second clone of MDCK cells transfected with rabbit plgR and human TfR (PTR10 cells) incubated with Tf and/or IgA and in a clone of MDCK cells transfected with the rabbit plgR alone (T23 cells) incubated with IgA (data not shown).

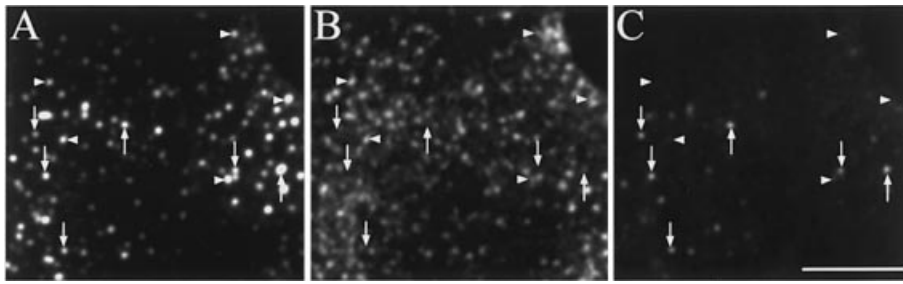


Figure 4: The overlap of fluorescence of vesicular dil-LDL with tubular OG-Tf corresponds to the physical accessibility of dil-LDL to HRP-Tf. Glass-grown cells were incubated for 15 minutes with dil-LDL, OG-Tf and HRP-Tf and fixed. A vertical series of images of the dil-LDL and OG-Tf fluorescence from a field of cells was then collected (projected in Panels A and B, respectively). The dish was then treated with DAB and peroxide for 2 minutes and a second vertical series of images of from the same field was collected. The projected image of dil-LDL following DAB/peroxide treatment is shown in panel C. Arrows indicate dil-LDL-containing compartments that are depleted in OG-Tf and resistant to HRP-mediated quenching. Arrowheads indicate dil-LDL-containing endosomes whose fluorescence overlaps with that of OG-Tf and are efficiently quenched by addition of DAB/peroxide. The scale bar is 10 μm in length.

Depolymerization of microtubules by prior incubation of cells in 33 μM nocodazole inhibited apical transport of LDL and Tf, stranding the two ligands at the lateral and basal membranes. Surprisingly, however, microtubule depolymerization also blocked the infiltration of LDL and Tf away from the basolateral plasma membrane and particularly blocked the formation of Tf-containing tubules (Figure 3K and L, respectively). Similar results were found in studies of living cells (not shown) and cells labeled with a combination of Tf and IgA (see below).

Physical relationship between sorting and recycling endosomes

The micrographs shown in Figure 3 frequently show a tubular pattern of IgA or Tf fluorescence that overlaps a sharply punctate LDL fluorescence. In order to establish that these

optical colocalizations represent physical continuity between the vesicular LDL and tubular Tf compartments, we used a biochemical assay in which the physical colocalization of HRP-Tf and dil-LDL is indicated by the HRP-mediated quenching of dil fluorescence upon addition of DAB and hydrogen peroxide. Cells grown on glass coverslips were incubated for 15 minutes with dil-LDL, OG-Tf and HRP-Tf and fixed. A vertical series of images of the dil-LDL and OG-Tf fluorescence from a field of cells was collected. The dish was then treated with DAB and peroxide for 2 minutes and a second vertical series of images of the same field was collected.

Projections of the vertical series of images from a representative field are shown in Figure 4. Panels A and B show the initial fluorescence of dil-LDL and OG-Tf, respectively, while

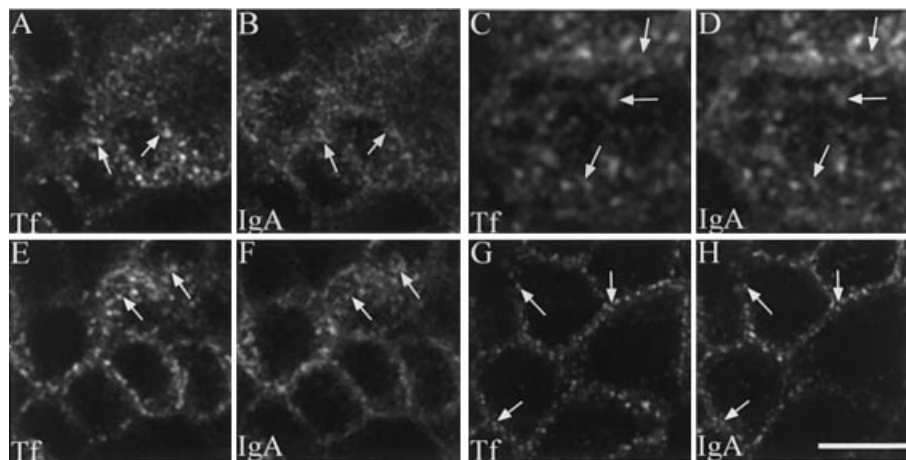


Figure 5: IgA and Tf are sorted to the same recycling endosomes. After 10 minutes of continuous incubation, Tf and IgA are found colocalized in both vesicles and tubules distributed throughout the cell. Panels A and B – A supranuclear focal plane showing TxR-Tf and OG-IgA fluorescence of a field of cells incubated for 10 minutes. Panels E and F – A corresponding pair of images collected 1.6 μm lower, at the level of the nuclei. Panels C and D – High magnification images of fields labeled with TxR-Tf and OG-IgA. Panels G and H – A medial focal plane of cells incubated for 15 minutes with TxR-IgA and OG-Tf, after prior treatment for 1 h in 33 μM nocodazole. Arrows indicate examples of compartments containing both Tf and IgA, which are frequently tubular, except in nocodazole-treated cells. The scale bar reflects a length of 15 μm for all panels, except C and D where it reflects 7.5 μm .

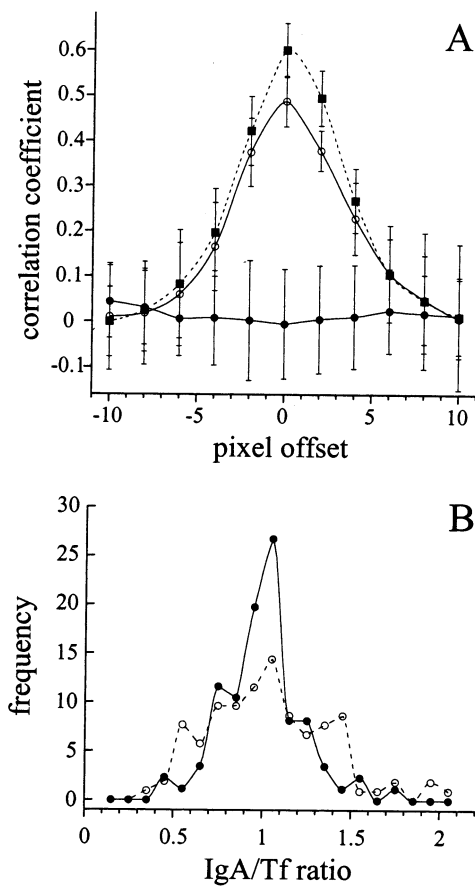


Figure 6: IgA and Tf are proportionally sorted to the same recycling endosome. A: Cross correlation analysis of the distribution of Tf and IgA in cells labeled for 10 minutes with OG-IgA and TxR-Tf (open circles, n = 10) or with OG-Tf and TxR-Tf (closed squares, n = 5). For comparison, the correlations for images of OG-IgA compared with a vertically inverted image of TxR-Tf (closed circles, n = 10) are also shown. The details of this analysis are described in detail in Materials and Methods. B: Quantification of sorting of Tf from IgA in sorting endosomes. Polarized cells were incubated with basolateral OG-IgA, TxR-Tf and diD-LDL for 10 minutes, rinsed and fixed. Fluorescence images were collected at medial focal planes and analyzed as described in Materials and Methods and the ratio of IgA/Tf in sorting endosomes containing diD-LDL (closed circles) or recycling endosomes lacking diD-LDL (open circles) was quantified. Ratios were standardized such that the mean ratio of sorting endosomes (containing diD-LDL) for each cell was 1.0 and the data pooled. For sorting endosomes containing diD-LDL, mean IgA/Tf = 1.00 ± 0.23 , n = 86, for recycling endosomes lacking diD-LDL, mean = 1.04 ± 0.34 , n = 104.

Panel C shows the diI-LDL fluorescence of this field following treatment with DAB/peroxide. Arrows indicate compartments containing diI-LDL, whose fluorescence is relatively unaffected (compare Panels A and C). Careful examination of panel B shows that these compartments, which we interpret as late endosomes, are depleted of Tf, some corresponding to 'holes' in the Tf fluorescence pattern, some immediately

adjacent to compartments whose diI fluorescence has been effectively quenched. In contrast, endosomes whose diI-LDL fluorescence has been quenched by DAB/peroxide (arrowheads) show overlap in the patterns of OG-Tf and diI-LDL fluorescence. In some cases the overlap is nearly complete, while in others the OG-Tf fluorescence appears to extend along a tubule extending from the diI-LDL-containing vesicle.

These studies validate the optical colocalizations, demonstrating that optical overlaps between tubular recycling endosomes and vesicles containing LDL closely correspond to physical connections between the two. These results support the interpretation that some of the recycling endosomes containing Tf extend as tubules from vesicles containing LDL. However, not all recycling endosomes show an obvious optical overlap with LDL (Figure 3) and it is unclear whether these compartments are truly separate, or also connected to sorting endosomes, directly or indirectly.

Tf and IgA are jointly sorted from LDL to recycling endosomes

When cells are labeled for 10 minutes with both TxR-Tf and OG-IgA, a striking colocalization of the two probes is found. Figure 5 shows images of a field of cells incubated for 10 minutes in TxR-Tf and OG-IgA, collected at both a supranuclear focal plane (panels A and B, respectively) and a medial focal plane (panels E and F, respectively). At either focal plane, Tf and IgA colocalize in both vesicles and apparently tubular endosomes. The close colocalization of Tf and IgA in the supranuclear region of cells is more obvious in the higher magnification pair of images shown in Figure 5C and D. As with the transport of LDL and Tf described above, the movement of Tf and IgA apically and away from the lateral membranes into tubular recycling endosomes appears to depend upon microtubules, as it is completely sensitive to nocodazole (Figure 5G,H).

The time series experiments demonstrate that Tf and IgA move from vesicular sorting endosomes containing LDL to recycling endosomes lacking LDL. The extensive overlap of Tf and IgA in sorting and recycling endosomes is consistent with the model of default sorting in which the two are jointly transported from sorting endosomes to recycling endosomes. However, more stringent predictions of this model are that: 1) The distributions of Tf and IgA will not only overlap but their fluorescence intensities will be spatially correlated with one another; and 2) Tf and IgA will not only colocalize in both sorting endosomes and recycling endosomes, but will colocalize in constant proportions. Tests of these predictions are presented below.

We assessed the spatial correlation of the distributions of Tf and IgA by quantifying correlation coefficients between images of Tf and IgA fluorescence. Correlation coefficients reflect not only probe overlap, but also the correlation of the intensities of the two probes where they overlap (28). In this test, the matrix of fluorescence intensities of a 30 x 30 pixel region of one image is compared with that of a comparison image and a correlation coefficient calculated. By spatially

offsetting one image relative to the other, a range of correlation coefficients can be calculated. Uncorrelated images show a low correlation coefficient and lack of an obvious maximum at the point of zero image offset.

Figure 6A presents the results of this correlation analysis. An analysis of images of cells incubated for 10 minutes with OG-Tf and TxR-Tf provides a standard of maximal probe colocalization. As expected, a maximum correlation occurs at

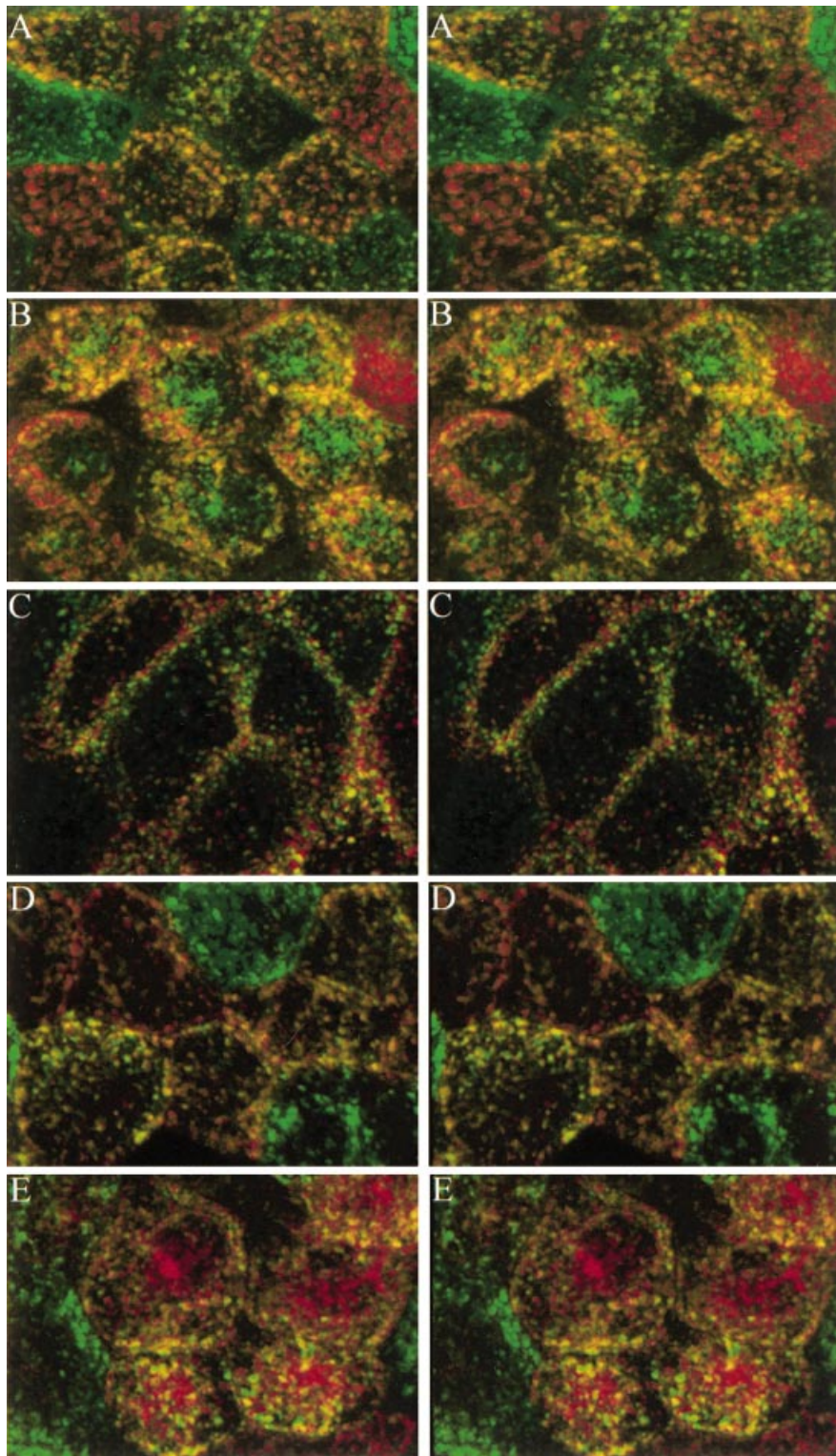


Figure 7: IgA initially colocalizes with Tf, but is subsequently sorted to an apical compartment depleted in Tf.

A: Stereopair images of cells fixed after incubation with TxR-Tf (red) and OG-IgA (green) for 10 minutes show an extensive and proportional colocalization of Tf and IgA throughout the cells. **B:** Cells incubated for 15 minutes with OG-IgA (green) and TxR-Tf (red) demonstrate that IgA is subsequently sorted from Tf to an apical compartment. **C:** Cells labeled for 15 minutes with OG-Tf (green) and TxR-IgA (red) after prior treatment for 60 minutes in 33 μM nocodazole show no apical transport of either Tf or IgA. **D:** Cells incubated with OG-Tf (green) for 15 minutes, with TxR-IgA (red) included for the last 5 minutes show no indication of an apical, IgA-enriched compartment. **E:** Cells incubated for 15 minutes with OG-Tf (green), with TxR-IgA (red) included for 5 minutes, then chased for 5 minutes show that during the 5 minutes chase IgA is sorted to the apical compartment. Scale bars were omitted from this figure as they interfere with stereo image formation. The field in panel A is 47 μm in height, B and C are 38 μm in height, D and E are 25 μm in height. Note that these stereopair figures are also represented as movies of rotated projections on the website located at <http://journals.munksgaard.dk/traffic/videogallery>

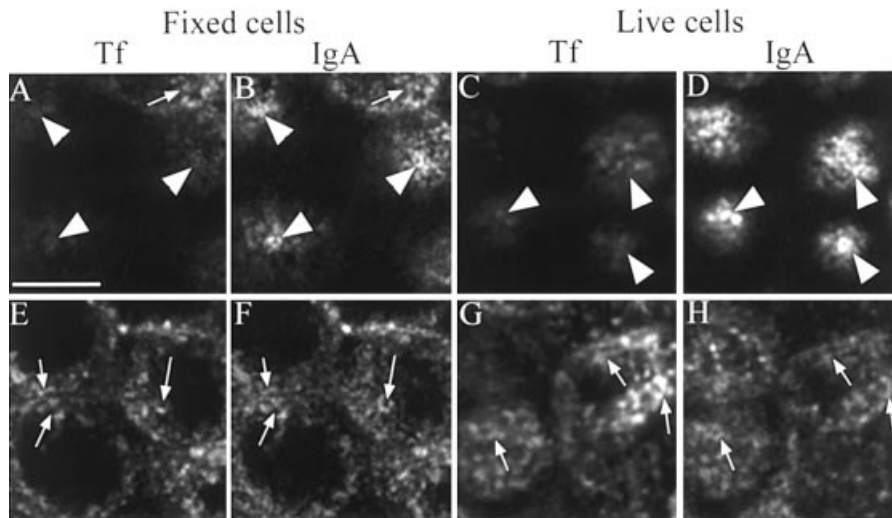


Figure 8: After 15 minutes of continuous incubation with both TxR-Tf and OG-IgA, IgA is found in an apical compartment depleted in Tf. An apical focal plane showing TxR-Tf and OG-IgA fluorescence of a field of cells incubated for 15 minutes is shown in panels A and B, respectively. A corresponding pair of images collected 3.0 μm lower, at the level of the nuclei is shown in panels E and F. Panels C, D, G and H: Live cells imaged in presence of OG-IgA and TxR-Tf, collected at the cell apex (C and D) or 1.2 μm lower (G and H). AREs depleted of Tf and enriched in IgA are denoted with arrowheads, while examples of recycling endosomes containing both Tf and IgA are denoted with arrows. The scale bar represents 10 μm length.

the position of zero offset, at a value of approximately 0.6. Similar results are obtained in an analysis of images of cells labeled for 10 minutes with OG-IgA and TxR-Tf, with a maximum correlation coefficient of 0.5. For comparison, an analysis of uncorrelated images is also presented, showing a correlation coefficient of zero for all offsets. It is clear from these results that the spatial correlation of Tf and IgA fluorescence after 10 minutes of internalization is nearly as high as that between two different conjugates of Tf.

In order to test whether Tf and IgA are transported from sorting endosomes to recycling endosomes in a constant proportion, we compared the ratio of IgA to Tf fluorescence in sorting endosomes to that in recycling endosomes. For this analysis cells were labeled for 10 minutes with basolateral OG-IgA, TxR-Tf and diD-LDL (a far-red fluorescent LDL otherwise similar to diI-LDL). For each of 33 cells, IgA and Tf fluorescence was measured in several sorting endosomes (containing LDL) and several recycling endosomes (with a distinctive tubular morphology and lacking LDL). IgA/Tf fluorescence ratios of individual sorting and recycling endosomes were calculated and then standardized such that the mean sorting endosome IgA/Tf ratio in each cell was 1.0 and the data were pooled. In Figure 6B, the results of this analysis show that the ratio of IgA to Tf in sorting endosomes is nearly identical to that in recycling endosomes (1.00 vs. 1.04).

Comparisons of the single focal plane images shown in Figure 5 demonstrate the precise colocalization of IgA and Tf during the first 10 minutes of incubation, but the similar cellular distributions of the two are more apparent in the 3-dimensional color stereopair images of Figure 7A. Although

the monolayer shows a mosaic appearance, reflecting the variable relative expression of pIgR and TfR, the nearly constant color of the endosomes in each cell reflects not only the similar distribution of IgA and Tf, but also the similar proportion of the two in endosomes throughout the cell.

Taken together, these results demonstrate that after 10 minutes of incubation, Tf and IgA are sorted from LDL, but

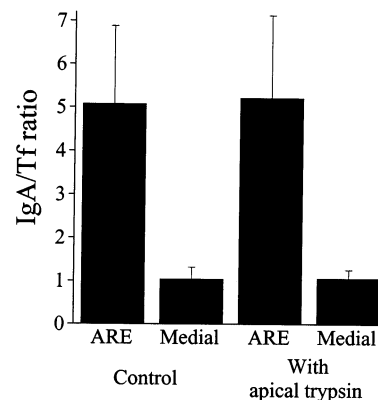


Figure 9: Quantification of intracellular sorting of IgA from Tf. Cells were incubated with basolateral OG-IgA and TxR-Tf for 15 minutes in the presence or absence of 100 $\mu\text{g}/\text{ml}$ of trypsin in the apical medium, a treatment determined to efficiently strip apically exposed IgA from cells. For each cell, IgA/Tf ratios were calculated for AREs and recycling endosomes collected 4–5 μm lower and standardized as described in Materials and Methods. For control cells, ARE mean IgA/Tf = 5.07 ± 1.92 , $n = 19$, recycling endosome mean 1.04 ± 0.20 , $n = 76$. For trypsin-treated cells, ARE mean IgA/Tf = 5.21 ± 1.81 , $n = 8$, recycling endosome mean 1.06 ± 0.28 , $n = 30$.

not from one another. Consistent with the model of default sorting, the distributions of IgA and Tf not only overlap, but are quantitatively similar by two different criteria.

IgA is sorted from Tf prior to delivery to the ARE

Between 10 and 15 minutes of basolateral incubation, fluorescent IgA is directed to the extreme apical pole of the cell to a structure similar to that previously described as the ARE (4,23). We have observed this structure in PTR9 cells, PTR10 cells and T23 cells. Consistent with the results of Barroso and Sztul (23) we find that this apical compartment is notably deficient in Tf. Figure 7B shows a color stereopair image of cells labeled for 15 minutes with both TxR-Tf and OG-IgA. The ARE of each cell is apparent as a green apical cap labeled with OG-IgA alone, while the yellow-to-orange endosomes in lower focal planes reflect the extensive colocalization of the green IgA with red Tf in recycling endosomes. The profound enrichment of IgA in the ARE is especially apparent in one particular cell at the top right of this field that has clearly internalized more TxR-Tf (red) than OG-IgA (green), but nonetheless shows an apical cap of IgA alone. A similar depletion of Tf in the ARE was found in the PTR10 cell clones (data not shown).

We have verified that this apical concentration occurs in an intracellular compartment, rather than reflecting a concentration of uncleaved plgR-IgA complexes at the apical plasma

membrane. The compartment is acidified and inaccessible to extracellular antibodies (Wang et al., in preparation). The apical accumulation is also insensitive to the presence of trypsin in the apical medium (see below).

Previous studies have shown that apical transport of IgA requires intact microtubules (4,29). We find that microtubules are necessary for apical transport of both Tf and IgA, as prior incubation of cells in 33 μ M nocodazole left both OG-Tf (green) and TxR-IgA (red) arrayed in punctate endosomes adjacent to the lateral and basal membranes (Figure 7C).

The sequential itinerary of IgA from recycling endosomes containing Tf, to the ARE lacking Tf is demonstrated in pulse-chase experiments. In the first experiment, cells were incubated with OG-Tf for 15 minutes, with TxR-IgA included for the final 5 minutes. In the second, cells were incubated with Tf for 5 minutes, both Tf and IgA for 5 minutes and finally with Tf alone for the final 5 minutes. The color stereopair shown in Figure 7D shows that after 5 minutes of incubation, TxR-IgA (red) colocalizes extensively in medial endosomes with OG-Tf (green) yielding a constant color to the endosomes in each cell, with little indication of ARE localization. As mentioned previously, differences between cells in the color of the combined fluorescence of TxR-IgA and OG-Tf reflects the relative expression of the two trans-

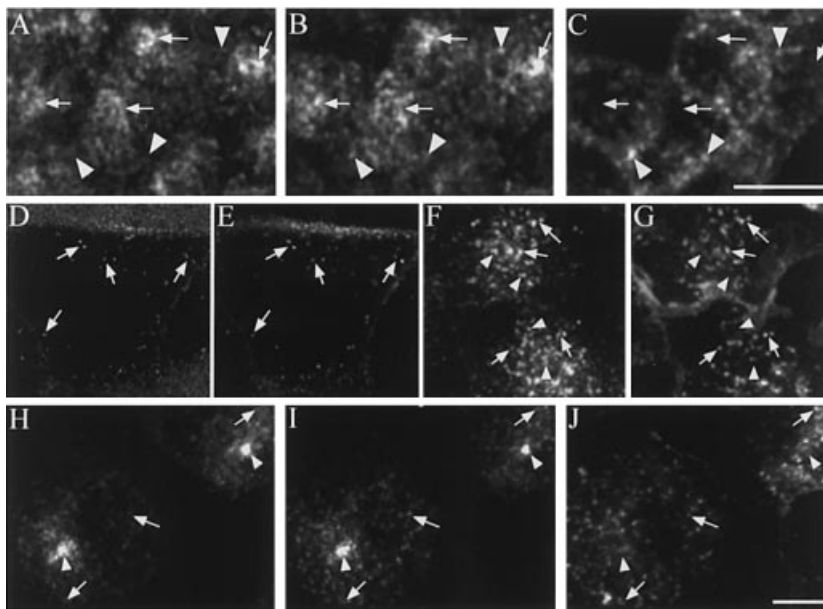


Figure 10: Rab11 is associated with a post-sorting IgA-containing compartment in both polarized and non-polarized cells.

Panels A–C: Distribution of immunolocalized rab11 (A) in a projected image volume of polarized cells labeled for 20 minutes with TxR-IgA (B) and Alexa-Tf (C). Arrows denote compartments containing rab11 that are enriched in IgA, while arrowheads indicate compartments containing Tf, but lacking rab11. Panels D and E: live, glass-grown cells imaged in presence of rhodamine-IgA and Cy5-Tf, within a few minutes of incubation show complete colocalization of IgA and Tf (arrows indicate examples). Panels F and G: Live, glass-grown cells imaged in presence of TxR-IgA and OG-Tf, after 15 minutes of incubation show sorting of IgA to compartments lacking Tf (arrowheads indicate examples). Panels H–J: Distribution of immunolocalized rab11 (H) in a projected image volume of glass-grown cells labeled for 20 minutes with TxR-IgA (I) and Alexa-Tf (J). Arrowheads indicate compartments containing rab11 that are enriched in IgA and depleted of Tf, while arrows indicate Tf-containing compartments with little rab11 labeling. Scale bars are 10 μ m in length, with the bar in C pertaining to panels A–C, the bar in J pertaining to the remaining panels.

ected receptors. The color stereopair shown in Figure 7E shows that with a subsequent 5 minutes chase, much of the TxR-IgA is directed to the ARE, which now appears as a red apical structure.

Although color stereopair projections present the 3-dimensional distribution of Tf and IgA, the endosome morphology and the relative distributions of Tf and IgA can be more precisely assessed by comparing separate images of each probe. Figure 8 shows single focal planes from a portion of the field of cells shown in Figure 7B, which were incubated for 15 minutes with TxR-Tf and OG-IgA. Because of differences in cell height, the AREs are more apparent in the color projections, but in apical optical sections the enrichment of OG-IgA in the ARE (arrowheads, Panel B) relative to TxR-Tf (Panel A) is apparent. This enrichment is more obvious considering that the levels of fluorescence of the two ligands in the recycling endosomes of the medial planes are relatively similar (Panels E and F). These images also demonstrate the pronounced colocalization of Tf and IgA in the recycling endosomes that distribute above and around the nucleus (arrows). Images of living, polarized cells confirm the depletion of Tf in the ARE (panels C and D) as well as the extensive colocalization of Tf and IgA in recycling endosomes in medial planes (panels G and H).

Studies in which cells were incubated basolaterally for 15 minutes with dil-LDL and OG-IgA showed that although many of the LDL-containing compartments are located in the supranuclear regions of cells, the ARE is completely lacking LDL (data not shown).

Quantification of sorting of IgA from Tf

We used digital image analysis to quantify the enrichment of IgA in the ARE. Cells were incubated with basolateral OG-IgA and TxR-Tf for 15 minutes and then fixed. As described in Materials and Methods, complete image volumes were collected and the ratio of IgA/Tf fluorescence of AREs and recycling endosomes imaged 3–4 μm lower in the same cell were measured. Data were standardized such that the mean recycling endosome ratio for each cell was 1.0 and pooled. As shown in Figure 9, we found a 5-fold enrichment of IgA relative to Tf occurs in the transport from the medial compartments to the ARE.

While we have interpreted the enrichment of IgA in the ARE as the consequence of sorting of IgA from Tf in recycling endosomes, it is also possible that both Tf and IgA are directed to the ARE, but IgA accumulates in the ARE due to futile recycling at the apical plasma membrane. In order to test this possibility, parallel samples of cells were incubated in the presence of 100 μg/ml of trypsin in the apical medium. As previously found (4), control experiments showed that this treatment rapidly strips IgA exposed at the apical membrane before it can become internalized (see Materials and Methods). Figure 9 shows that a similar enrichment of IgA in the ARE was observed in the presence apical trypsin (5.1-fold vs. 5.2-fold), demonstrating that IgA enrichment occurs prior to delivery to the apical plasma membrane.

The 5-fold enrichment of IgA relative to Tf in the ARE found in our single-cell sorting assays mirrors the biochemical measurements of the relative rates of IgA and Tf transcytosis in monolayers (Figure 1). Taken together with the previous analyses showing a lack of polar sorting between sorting endosomes and the recycling endosomes, these measurements indicate that all polar sorting occurs between the recycling endosomes and the ARE.

Rab11 is associated with Tf-depleted compartments

Previous studies have associated the small GTP-binding protein rab11 with an apical endosome of gastric parietal cells (17,30) and with the ARE of MDCK cells (16). Using immunofluorescence to localize rab11, we have determined that rab11 is associated with the ARE as defined in our studies, that is with an apical compartment enriched in transcytotic IgA, but depleted of Tf. Figure 10 shows a projected image volume of cells incubated with fluorescent Tf and IgA for 20 minutes and then processed for rab11 immunofluorescence. In each cell one sees rab11 (panel A) associating with the ARE heavily labeled with IgA (panel B) and lacking Tf (panel C) (noted with arrows). Indeed the distribution of rab11 is the opposite that of Tf, with rab11 localizing to the empty spaces of the Tf image and depleted or missing from the dispersed compartments containing Tf, most of which also contain IgA (arrowheads).

This pattern contrasts strikingly with that of previous studies of fibroblasts showing rab11 prominently associated with the

Table 1: Properties of the three endocytic compartments of the transcytotic pathway of MDCK cells

	Sorting endosomes	Recycling endosomes	Apical recycling endosomes
Enriched ligands	IgA, Tf, LDL	IgA, Tf	IgA
Cellular distribution	Medial and largely lateral	Extensive, throughout apical and medial cytoplasm	Centered at extreme apical
Rab11	Absent?	Depleted	Enriched
Accessible to apical membrane probes?*	No	Yes	Yes
Morphology	Vesicular	Tubular	Tubular
Microtubule-dependent distribution?	No	Yes	Yes
pH*	5.8	5.8	6.5

* Data provided by Wang et al. (in preparation).

Tf recycling compartment (22,26,31,32). In order to determine whether this difference reflects changes that accompany the development of membrane polarity, studies were performed using flat PTR cells shortly after seeding onto a solid substrate. Although such cells ultimately form domes and display a limited polarized phenotype, subconfluent MDCK cells are characterized by a lack of plasma membrane polarity (33,34). PTR cells grown in this way show a flat morphology and internalize Tf and LDL from their upper surface, reflecting a lack of membrane polarity. Images of living cells collected within a few minutes of exposure to fluorescent IgA and Tf (Figure 10D and E, respectively), show that both ligands are initially internalized into the same endosomes (arrows). Surprisingly, however, these cells are clearly capable of efficient polarized sorting; with subsequent incubation, IgA is directed to endosomes lacking Tf, as shown in the images of living cells shown in panels F and G (arrowheads).

As with polarized cells, the post-sorting IgA-containing compartment of flat, glass-grown cells is prominently associated with rab11. Although this compartment frequently lacks the condensed morphology seen in fully polarized cells (e.g. Figure 10F,G), Figure 10H–J show an example of a field of cells in which rab11 (panel H) strongly associates with condensed compartments enriched in IgA (Panel I), but lacking Tf (Panel J). As with polarized cells, compartments containing Tf and IgA show minimal rab11 immunofluorescence (arrows). Thus, in contrast to fibroblasts, rab11 is not associated with the Tf recycling pathway of MDCK cells, rather it is predominately associated with the compartments to which IgA is directed after sorting from Tf.

Discussion

In order to dissect the relationship between lysosomal and polarized sorting of plasma membrane proteins, the endocytic itineraries of LDL, IgA and Tf were analyzed and compared in an MDCK cell line expressing the rabbit pIgR and human TfR. To assure that the observations apply to polarized cells, the characterizations of endocytosis in polarized cells described here were conducted on filter-grown cells whose polarity was established by a variety of criteria. Unique 3-dimensional morphological characterizations, combined with microscopic single-cell sorting assays allowed us to determine the sites and efficiencies of intracellular sorting. A simple method for microscopic analysis of living, filter-grown cells allowed us to characterize the morphology and physiology of endosomes in living cells, thereby verifying the biological validity of our observations.

Summary — sequential endocytic sorting in polarized MDCK cells

These studies demonstrate that Tf, IgA and LDL are internalized into a common population of punctate lateral sorting endosomes. Within a few minutes, Tf and IgA are jointly sorted from LDL into recycling endosomes distributed throughout the apical and lateral cytoplasm. Within 10 to 15 minutes of internalization, IgA is transported from recycling

endosomes to the ARE at the apex of the cell, as has been previously observed (4,23). Although Tf is also transported to this compartment, it is depleted 5-fold relative to IgA. The agreement between this sorting efficiency and the relative efficiency of transcytosis of IgA and Tf in these cells indicates that polar sorting is completed in recycling endosomes prior to delivery of IgA to the ARE. Interestingly, polar sorting does not require development of plasma membrane polarity. Glass-grown cells, whose lack of membrane polarity is demonstrated by their uptake of Tf and LDL from their upper surface, were found to efficiently sort IgA from Tf.

The data presented here support a model of sequential endocytic sorting in which basolaterally internalized membrane proteins are first jointly sorted from lysosomally directed ligands into a set of microtubule-dependent recycling endosomes distributed throughout the cell. While basolateral membrane proteins recycle from recycling endosomes, apical membrane proteins are sorted to the ARE. Recent results demonstrate that the recycling endosomes are also widely accessible to IgA internalized from the apical plasma membrane (Wang et al., in preparation), indicating that recycling endosomes conduct polar sorting for both the apical and basolateral endocytic pathways. These recent results also suggest that the recycling endosomes identified here may be equivalent to the 'common endosomes' previously observed in MDCK and Caco-2 cells by Hopkins et al. (5,6,19,35).

The transport sequence presented here represents the sorting itinerary of MDCK cells, but not necessarily all of the intracellular fluxes. Sheff et al. (15) has demonstrated that a significant fraction of Tf and IgA effluxes from cells directly from sorting endosomes, without being sorted from one another. This process is fundamentally similar to a rapid recycling process previously observed in a variety of cells (reviewed in (36)).

Default membrane-volume sorting in polarized MDCK cells

Previous studies of fibroblasts support the model in which receptor recycling is accomplished through a default process of membrane-volume sorting in sorting endosomes (9,10). Consistent with this model, we find that MDCK cells sort both Tf and IgA from vesicular sorting endosomes into recycling endosomes. However, a stronger test of the default model of endocytic sorting comes from the simple prediction that different membrane proteins will be sorted from the sorting endosome in identical proportions. This prediction was previously tested and demonstrated in comparisons of Tf and lipid trafficking in fibroblasts (9). PTR cells provide an excellent system to perform a similar test of this prediction as they permit comparison of Tf and IgA, membrane probes with different ultimate cellular fates. Quantitative analyses demonstrate that IgA and Tf are sorted identically from sorting endosomes containing LDL, to recycling endosomes lacking LDL. Sheff et al. (15) and Verges et al. (14) recently obtained similar results, although the fractionation techniques used in their studies resolved only a single downstream compartment.

MDCK cells manifest several other characteristics consistent with this default mechanism. Recent work from our laboratory indicates that basolateral sorting endosomes are acidified to a similar degree as the sorting endosome of CHO cells (Wang et al., in preparation), a pH sufficient to dissociate ligands from their receptors (reviewed in (37)). Recent studies also indicate that while LDL accumulates in sorting endosomes over an extended period, Tf rapidly fluxes through sorting endosomes (data not shown), reflecting an iterative sorting process similar to that observed in non-polarized cells (10,38).

Physical relationship between sorting and recycling endosomes

The exclusion of LDL from recycling endosomes containing both Tf and IgA functionally distinguishes them from sorting endosomes, but the physical relationship between the two is less clear. Many recycling endosomes appear to extend from sorting endosomes containing LDL. This observation is consistent with previous ultrastructural studies of rat liver cells (11) and glass-grown MDCK cells (25), which indicate that recycling endosomes arise as tubular extensions of sorting endosomes. While fluorescence microscopy is unable to resolve physical connections between adjacent compartments, fluorescence quenching experiments indicate that the optical overlap observed between many recycling and sorting endosomes reflects a physical continuity.

Gibson et al. (25) present stunning fluorescence and electron micrographs of an interconnected network of tubular and vesicular endosomes in glass-grown MDCK cells. While these authors find that endosome tubulation occurs only in the presence of IgA, we find no difference in the extent or distribution of endosome tubules in cells incubated with Tf or IgA or both (compare Figures 3 and 5). This is an important difference in that, as discussed above, endosome tubulation is a critical component of the default model of endocytic sorting and one would not expect efficient recycling of Tf to depend upon the presence of IgA. This discrepancy may reflect differences in method. While our studies were conducted using polarized, filter-grown cells continuously maintained at 37°C, the lengthy IgA-dependent tubules identified by Gibson et al. (25) were observed in glass-grown cells and were induced by shifting cells to 37°C after a protracted incubation at 20°C.

Similar to previous studies (11,25), we also detected recycling endosomes with no obvious connection to sorting endosomes, indicating that recycling endosomes may ultimately detach from sorting endosomes to form distinct compartments. A distinct recycling endosome fraction is resolved by gradient fractionation of MDCK cells (14,15), but may reflect a fragmentation that occurs during isolation.

Two distinct membrane recycling compartments in MDCK cells

Our observation that polar sorting occurs downstream of the basolateral sorting endosome is consistent with several pre-

vious studies which, likewise, place polar sorting in a downstream compartment (4,14,15,25). However, our studies are unique in that they localize polar sorting to the first of two downstream membrane recycling compartments, the first transited by both Tf and IgA, the other transited almost exclusively by IgA. The distinction is important to interpreting previous studies of endocytic sorting in MDCK cells and particularly to interpreting studies of the ARE.

The ARE has been the focus of much recent research, with various studies implicating functions in polarized sorting, lysosomal sorting, regulated secretion and disease processes (reviewed in 18). Studies have localized various rabs to the ARE, including rab11a (16,17), rab17 (21,39) and rab25 (16) and these associations have been used to try to understand the functions of both the ARE and the particular rab proteins.

Interpreting these studies is complicated by the fact in each case a single ARE-like endosome is identified using criteria that would not distinguish the two functionally and physically distinct compartments found in the apical cytoplasm of MDCK cells — the ARE and the recycling endosomes. Each study employed various combinations of the following criteria to define an ARE: an apical endosome, whose structure and distribution is dependent upon microtubules, positioned downstream of a microtubule-dependent step in apical transcytosis, accessible to both apical and basolateral endocytic probes and localized adjacent to centrioles. Our studies demonstrate that these characteristics are shared by both the recycling endosomes and the ARE. Both compartments are found in the apical cytoplasm, in both cases their structure and apical distribution depend upon microtubules and recent studies (Wang et al., in preparation) demonstrate that both are accessible to IgA internalized either apically or basolaterally. Our images of the ARE indicate that it corresponds well to the pericentriolar structure identified in Apodaca et al. (4) and Casanova et al. (16). However, since both compartments are found in close proximity in the apical cytoplasm, pericentriolar localization in itself will not discriminate between the ARE and the recycling endosomes.

Our studies have identified several new criteria that clearly distinguish the ARE and recycling endosomes. First, quantitative confocal microscopy demonstrates that the recycling endosomes contain Tf and IgA in equal proportion to that found in basolateral sorting endosomes, while the ARE is 5-fold enriched in IgA relative to Tf. Second, the recycling endosomes distribute throughout the apical and lateral cytoplasm, while the ARE is localized at the extreme apical pole of the cell. Third, rab11 is predominately and closely associated with the extreme apical ARE. Fourth, recent studies from our laboratory demonstrate that the recycling endosomes are acidified to a pH of 5.8, while the ARE is nearly neutral, with a pH of 6.5 (Wang et al., in preparation). In addition to being functionally distinct, the sharp demarcations of IgA/Tf ratios and pH indicate that the ARE is physically distinct from other endocytic compartments. These distinc-

tions have proven to be robust, apparent in cells incubated for varying lengths of time, incubated with IgA from both sides of the monolayer, with various combinations of fluorescent probes and most importantly, in living cells.

Thus, the transcytotic pathway of MDCK cells consists of three distinct stations, the basolateral sorting endosomes shared by IgA, Tf and LDL, the recycling endosomes containing IgA and Tf and the ARE in which IgA alone is enriched. The properties of these three compartments are summarized in Table 1. As discussed above, the physical distinction of recycling endosomes from sorting endosomes is unclear. We use the term 'recycling endosome' here because, regardless of their physical distinction, the recycling endosomes clearly represent a functionally distinct sorting station.

Relationship to previous studies of polarized sorting in MDCK cells

By distinguishing two apical membrane compartments downstream of sorting endosomes, our results provide a framework that may justify previously conflicting results as to the location of polarized sorting on the transcytotic pathway of MDCK cells.

Apodaca et al. (4) and Barroso and Sztul (23) both demonstrated that IgA is delivered to the ARE prior to apical efflux. Unlike Barroso and Sztul (23) however, Apodaca et al. (4) suggested that Tf is also transported through the ARE. This is an important difference, since the transport of Tf through the ARE implies that the ARE conducts polar sorting in MDCK cells. Our studies clearly demonstrate that polarized sorting occurs in the recycling endosomes prior to the ARE. The simplest explanation for these different findings is that, while the morphological studies of both Apodaca et al. (4) and Barroso and Sztul (23) detected the ARE, the extensive colocalization of Tf and IgA measured in the biochemical assays of Apodaca et al. occurred within the recycling endosomes. This interpretation is consistent with the suggestion of Apodaca et al. that the ARE, as originally defined, might consist of distinct subcompartments.

Recently, Sheff et al. (15) attributed polar sorting to the second of two compartments isolated by gradient fractionation, a fraction identified by a depletion of rab4 and enrichment of rab11. Although referred to as a 'recycling endosome' fraction, given the association of rab11 with the ARE shown here and elsewhere (16,17), this model would lend support to the idea of polar sorting in the ARE. However, in light of our results, it is likely that the single downstream compartment identified in these studies actually consists of a mixture of two distinct compartments, the first responsible for polar sorting, the second associated with rab11 and downstream of the polar sorting step.

Our results are most consistent with the ultrastructural studies of Gibson et al. (25), which indicated that some

degree of polar sorting in MDCK cells occurs in tubular extensions from sorting endosomes. However, our determination that polar sorting is complete prior to the ARE extends the results of this earlier study, which detected relatively low efficiency sorting in the tubular extensions and whose glass-grown cells lacked a discernible ARE. When put in the context of our studies of polarized cells, the vesicular process resolved in the electron micrographs of Gibson et al. (25) seems likely to underlie the polar sorting we observe in the recycling endosomes of polarized cells.

Given its terminal position on the apical membrane pathway, a likely function of the ARE appears to be to regulate the expression of apical plasma membrane proteins. IgA efflux from the ARE has been found to be regulated by second messengers (40). A rab11-associated compartment comparable to the ARE has been found to be responsible for regulated expression of H⁺-ATPase and K⁺-ATPase in gastric parietal cells (17,30).

Relationship between the ARE and the fibroblast PRC

Interest in the relationship between the endocytic pathways of polarized and non-polarized cells has been stimulated recently by the observation that the ARE of polarized cells shares many characteristics of the PRC of fibroblasts, including pericentriolar localization, microtubule-dependent organization, tubular morphology, terminal position in the recycling endocytic pathway and association with rab 11a and rab17 (4,16–18,20–22,39). Recent studies from our laboratory also show that the pH of the ARE is almost identical to that of the PRC, in both cases significantly higher than that of the endosomes preceding it (Wang et al., in preparation).

The putative homology between the PRC and ARE has been taken to suggest that the PRC, whose function has long been elusive, might be a cognate polar sorting compartment in fibroblasts (4,21). Cognate polar sorting pathways have previously been demonstrated along the biosynthetic pathway of fibroblasts (41,42). The possibility that the PRC is a cognate endocytic polar sorting compartment is supported by a recent study which shows that rab17, a rab protein induced during cell polarization, is both localized to the fibroblast PRC and involved in polarized membrane sorting in an epithelial cell line (21).

This attractive suggestion now seems untenable; our results not only demonstrate that the ARE is not responsible for polar sorting, but also complicate the interpretation of the ARE as homologous with the fibroblast PRC. First, while the majority of the Tf internalized by CHO cells is associated with and transported through the PRC (9,43), we find that the ARE experiences minimal Tf traffic. Second, while previous studies of fibroblasts that have shown rab11 prominently associated with the Tf recycling compartment (22,26,31,32), in MDCK cells we find rab11 primarily associated with a compartment to which IgA is directed after sorting from Tf. The fact that we find similar

polarized sorting and association of rab11 with sorted IgA in polarized and glass-grown MDCK cells indicates that these differences do not reflect the development of cell polarity, but rather suggest that there are significant differences between the fibroblast PRC and the MDCK ARE. Furthermore, the lack of association of rab11 with Tf-containing endosomes of MDCK cells indicates that rab11, previously demonstrated to regulate Tf recycling in fibroblasts (22,26), performs different functions in fibroblasts and MDCK cells.

Materials and Methods

Cell lines

MDCK strain II cells used in these studies were transfected with both the human TfR and the rabbit plgR. A cDNA encoding human TfR (corresponding to nucleotides –30 to 2385 of TfR mRNA) cloned in the ClaI site of pbluescript SK (44) was excised with Sall and BamHI and ligated into Sall/BamHI cut pCB7 (45). DNA was purified on a Qiagen column and used to transfect MDCKII cells expressing rabbit plgR (46) by the calcium phosphate method. Stable clones were selected in the presence of 250 µg/ml hygromycin (Boehringer, Indianapolis, IN). Colonies were isolated using cloning cylinders and screened for TfR expression by western blotting with the H68.4 monoclonal antibody (47). Two transfected clones, referred to as PTR9 and PTR10 were used in this study. All of the data presented here were derived from studies of PTR9 cells, but many were repeated using PTR10 and T23 cells, another MDCKII cell line transfected with the rabbit plgR (48).

It was determined that 85% of the transfected human TfR is expressed on the basolateral membrane. For Tf polarity studies, polarized monolayers of cells were depleted of previously internalized Tf by incubation for 4 h in MEM/BSA (MEM containing Hank's balanced salts, 0.6% BSA and 20 mM HEPES, pH 7.4). Cells were then incubated from the basolateral or apical side with ¹²⁵I-Tf, prepared as previously described (4) for 2 h at 4°C. Filters were then washed rigorously and counted in a gamma counter. ¹²⁵I-Tf binding was found to be 95% compatible with excess unlabeled Tf. The specificity of the plgR was described previously for the parental cells (46).

Cell culture

PTR cells were grown in MEM (Life Technologies, Grand Island, NY) with 8% FBS, 1% L-glutamine, streptomycin and 0.05% hygromycin (Calbiochem, San Diego, CA). Cells were passed every 3–4 days and growth medium changed daily. New cultures of cells were thawed every 4–5 weeks. For fluorescence experiments, cells were plated at confluence on the bottoms of collagen-coated Millipore CM 12 mm filters and cultured for 4–5 days prior to experiments. At this point *trans*-epithelial resistance plateaued at 450 ohms cm² (after subtraction of 250 ohms cm² for the blank filter) as measured with a Millipore Millicell ERS resistance meter. Development of cell polarity was also indicated by the increase in cell height to between 12 and 18 µm, development of tight junctions (as assessed by immunofluorescence detection of the tight junction protein zo-1), 85% basolateral distribution of the TfR and by the minimal apical endocytosis of Tf. Monolayer impermeability was indicated not only by increased *trans*-epithelial resistance, but also by: 1) differences between the labeling patterns of apically and basolaterally internalized IgA (Wang et al., in preparation); 2) blockade of the normally extensive mixing of apically and basolaterally internalized IgA by microtubule depolymerization (Wang et al., in preparation); 3) restriction of extracellular labels and antibodies to the side of application and 4) uptake only the basolaterally applied form of Tf, when different conjugates of Tf were applied apically and basolaterally.

Cells labeled with fluorescent LDL were cultured in medium containing 8% lipoprotein-deficient medium to up-regulate the expression of the LDL receptor. Comparisons of the Tf or IgA labeling patterns of these cells with cells cultured in complete medium showed no effects on the morphology of endosomal compartments.

Biochemical assays of recycling and transcytosis

¹²⁵I-Tf and ¹²⁵I-IgA were prepared as described in (4). For Tf studies, cells were depleted of previously internalized Tf by incubation for 4 h in MEM/BSA. To assay ligand transcytosis and recycling, polarized monolayers of PTR9 cells were incubated from the basolateral side with ¹²⁵I-Tf for 2 h at 18°C or ¹²⁵I-IgA for 5 minutes at 37°C and then washed and re-incubated in the absence of radio-labeled ligand at 37°C. At various intervals cells were chilled and the apical and basolateral media collected. Surface Tf was stripped by incubation of cells in 750 mM glycine, pH 2.5 diluted 1:5 with PBS (supplemented with 0.5 mM MgCl₂ and 0.9 mM CaCl₂ for 1 h on ice. Filters were then cut out and radioactivity determined for the filters, the acid stripped fraction and for the basolateral and apical media.

Antibodies and proteins

Purified dimeric IgA was kindly provided by Professor J.-P. Vaerman (Catholic University of Louvain, Brussels, Belgium). Human Tf was obtained from Sigma Chemical Company (St Louis, MO), iron loaded and purified by S300 column purification as described in (49). Human LDL was obtained from Biomedical Technologies, Inc. (Stoughton, MA). Anti zo-1 antibody was obtained from the Developmental Hybridoma Bank (University of Iowa), rabbit anti-rab11 antibody from Zymed Laboratories (South San Francisco, CA) and anti-fluorescein antibody was obtained from Molecular Probes (Eugene, OR). With the exception of Cyanine 5.18 (Cy5) succinimidyl ester, which was obtained from Amersham Company (Arlington Heights, IL), all fluorescent probes were obtained from Molecular Probes. All other reagents were obtained from Sigma. Horseradish peroxidase conjugated to Tf (HRP-Tf) was obtained from Jackson ImmunoResearch (West Grove, PA).

Fluorescent ligand preparation

Fluorescent conjugates of Tf and IgA were prepared from succinimidyl esters of various fluorophores according to manufacturer's instructions. Oregon green 488 (OG) was added to Tf in a ratio of 12:1 and to IgA in a ratio of 16:1. Texas Red (TxR) was added to Tf in a ratio of 2:1 and to IgA in a ratio of 8:1. Fluorescein-ex (F) was added to Tf in a ratio of 8:1. Cy5 was conjugated to both Tf and IgA in a ratio of approximately 4:1. For a pH sensitive dye, Tf was conjugated to both fluorescein (F) and rhodamine (R) (F-R-Tf) in a ratio of 6:2:1.

Fluorescent LDLs were prepared as described in (50) with either 1,1'-dioctadecyl-3,3',3'-tetramethylindocarbocyanine perchlorate (dil) or 1,1'-dioctadecyl-3,3',3'-tetramethylindocarbocyanine perchlorate (diD), dialyzed against 150 mM NaCl with 0.01% EDTA, sterile filtered and stored under argon.

Labeling of cells with fluorescent ligands

For fluorescence labeling, cells were incubated at 37°C on a slide warmer in a humidified chamber for 15 minutes prior to addition of fluorescent ligands. All incubations were conducted in Medium 1 (150 mM NaCl, 20 mM HEPES, 1 mM CaCl₂, 5 mM KCl, 1 mM MgCl₂, 10 mM glucose pH 7.4). As described in each study, cells were labeled with 20 µg/ml fluorescent Tf, 20 µg/ml fluorescent LDL or 100 µg/ml fluorescent IgA. After incubations with fluorescence ligands, filters were rinsed briefly in PBS at 4°C, then incubated in 4% paraformaldehyde in PBS (pH 6.5) for 5 minutes, then transferred to 4% paraformaldehyde in 100 mM NaB₄O₇ (pH 11.0) for 10 min-

utes. Filters were then rinsed in PBS. The kinetics of endocytic labeling from the basolateral side were unaffected by the filter, as we found that the permeation rates of F-Tf and diL-LDL (the two extremes in size) through the filters are identical.

The specificity of receptor-mediated uptake of fluorescent LDL, IgA and Tf was demonstrated by its inhibition by competition with excess unlabelled ligands. Fluorescent IgA and Tf were both found to efflux the cells with kinetics similar to those of the radiolabeled ligands. Dual labeling experiments showed the endosomal distributions of ligands conjugated to different fluorophores to be identical.

The effectiveness of apical trypsin in stripping transcytosed IgA prior to reinternalization was demonstrated in control experiments in which cells were incubated for 60 minutes at 4°C with OG-IgA apically, rinsed and then incubated at 37°C for 15 minutes in the presence or absence of 100 µg/ml of trypsin in the apical medium. These experiments demonstrated that uptake was completely blocked when trypsin was included during the internalization (data not shown).

Immunofluorescence localizations

For immunolocalizations of rab11, cells were labeled with TxR Tf and Alexa488-IgA for 20 minutes at 37°C, then fixed as described above. Cells were then washed three times with PBS, pH 8.0 and incubated for 10 minutes in 75 mM NH₄Cl, 20 mM Glycine, pH 8.0 dissolved in PBS, pH 8.0 to quench nonreacted paraformaldehyde. The quenched cells were washed twice with PBS, pH 8.0 (5 minutes per wash) and nonspecific sites were blocked with PBS, 0.7% fish skin gelatin (FSG) and 0.025% (w/v) saponin (Sigma). The fixed cells were incubated in a humid chamber with 20 µg/ml rabbit anti-rab11 in PBS-FSG-saponin for 1 h at room temperature. Cells were then washed three times with PBS-FSG-saponin and once with PBS-saponin. Cells were rinsed once with PBS-FSG-saponin, then incubated for 1 h in a humid chamber with the secondary antibody, cy5-goat-anti-rabbit (Jackson ImmunoResearch) in PBS-FSG-saponin at room temperature. Finally, cells were rinsed three times with PBS-FSG-saponin, once with PBS-saponin and twice in PBS, pH 7.4 alone before imaging.

Microscopy

All experiments were conducted using a Bio-Rad MRC-1024 laser scanning confocal attachment mounted on a Nikon Diaphot 200 or Nikon Eclipse 200 inverted microscope using a Nikon 60X, N.A. 1.2 water immersion objective. Illumination is provided by a Krypton-Argon laser providing for fluorescence excitations at 488, 568 and 647 nm, allowing collection of up to three images simultaneously. In some experiments, potential bleed-through of the green channel into the red channel and of the red channel into the far-red channel required that images be collected sequentially, in which case no between-channel bleed-through was detected. Image volumes were collected by collecting a vertical series of images, each between 0.2 and 0.6 µm apart. Photomultiplier offsets were set such that background was slightly positive to guarantee signal linearity with fluorescence. Whenever possible signal saturation was avoided and objects with saturated pixels were omitted from quantifications.

As mentioned previously, cells were grown on the underside of Millipore filter units. After removing the legs of the filter units, living or fixed cells were observed by placing the entire filter unit on two 50-µm tape spacers attached to the coverslip of a coverslip-bottomed 35-mm dish (Mattek, Ashland, MA) mounted on the stage of an inverted microscope. For live cell studies, incubations are conducted in medium 1 on the microscope stage, with basolateral ligands added to the filter cup, while apical ligands are added to the well of the coverslip-bottomed dish. Temperature is maintained by a Medical

Systems Corporation PDMI-2 open perfusion chamber (Greenville, NY). Fixed cells were imaged immediately after fixation in PBS containing 2% DABCO (Sigma).

Image processing for presentation

Image processing was conducted using Metamorph software (Universal Imaging, West Chester, PA). In order to minimize photobleaching and phototoxicity in living cells, all fields were imaged with minimal averaging. To compensate, all images were subsequently averaged spatially using a 3 × 3 low pass filter. Images shown in figures were contrast stretched to enhance the visibility of dim structures and specific care was taken never to enhance the contrast in such a way that dim objects were deleted from an image. Different focal planes from the same field were contrast enhanced identically, except where noted. Montages were assembled and annotated using Photoshop (Adobe, Mountain View, CA).

Cross-correlation analysis

Cross correlation image analysis was conducted as described previously (28). Red and green fluorescence images of cells labeled with combinations of either OG-IgA and TxR-Tf or OG-Tf and TxR-Tf were collected sequentially as described previously, to guarantee no bleed-through of fluorescence from one fluorophore into the detector channel of the other. Regions were chosen for analysis independent of pattern of fluorescence, from the supranuclear region of cells in which the two probes showed similar levels of fluorescence. For each pair of images a 30 × 30 pixel region of one image from was compared with that of a comparison image and a Pearson's correlation coefficient (r_p) calculated as per the equation:

$$r_p = \frac{\sum(A_i - A_{av}) \cdot (B_i - B_{av})}{\sqrt{\sum(A_i - A_{av})^2 \cdot \sum(B_i - B_{av})^2}}$$

Where A_i and B_i are the intensity values of the pixel i of image A and B, respectively and A_{av} and B_{av} are the average pixel intensities of images A and B. The region was then shifted by a known distance relative to the comparison image and the correlation coefficient calculated again. The process is repeated for a range of offset distances. The proper performance of the test is indicated by the perfect correlation found between unshifted copies of the same image ($r = 1$, data not shown) and for the lack of correlation between vertically flipped versions TxR-Tf and OG-IgA image pairs ($r = 0$, Figure 6A). Since the analysis depends on representative labeling throughout the compared regions of the two images, both the region size and the regions selected for analysis were chosen so that the edges of the cells were avoided even with a maximum offset. Each analyzed region contained approximately 7–10 endosomes each.

Fluorescence ratio quantifications

Distinction of individual endosomes and quantification of endosome fluorescence was conducted as previously described (51). For endosome fluorescence ratio calculations, the common non-zero pixels for each endosome were determined and the fluorescence ratio within that region calculated. We guaranteed that sampling which was unbiased with respect to the measured ratio by using only one image of the image pair to identify clearly labeled and distinct endosomes for quantification. As much as possible, detector saturation was avoided during collection, but when pixel saturation occurred, objects with pixels within 10% of saturation (with a gray level of 230 or above in the original image) were removed from analysis. The methods used here are as described previously (8,52,53).

Endosome IgA/Tf ratios of recycling endosomes and AREs were determined from confocal images of cells labeled with both OG-IgA and TxR-Tf for 10–15 minutes. Cells with distinct AREs were iden-

tified and the total fluorescence of OG and TxR quantified for that region, as well as that of several recycling endosomes located 3–5 μm lower in the same cell. For each cell, the relative amounts of internalized IgA and Tf were standardized by multiplying the OG-IgA/TxR-Tf ratios of both the AREs and the recycling endosomes by a factor such that the mean IgA/Tf ratio of the recycling endosomes equaled one. After standardization, measurements from multiple cells were then pooled. Laser illumination levels were low so that photobleaching is estimated to have accounted for no more than 1% variation in fluorescence of AREs versus recycling endosomes.

Endosome IgA/Tf ratios of sorting endosomes and recycling endosomes were determined from confocal images of cells labeled with OG-IgA, TxR-Tf and diD-LDL (a far-red fluorescing form of LDL similar to diI-LDL) for 10 minutes. Images of medial planes were then collected and cells with sufficient IgA and Tf labeling to support quantification and sufficient LDL uptake to allow reliable identification of sorting endosomes were selected for analysis. For each cell a single focal plane was chosen and several endosomes containing Tf, IgA and LDL (sorting endosomes) or containing Tf and IgA, but no detectable LDL (recycling endosomes) were identified and the OG-IgA and TxR-Tf fluorescence quantified for each. As above, the relative amounts of internalized IgA and Tf were standardized for each cell by multiplying the IgA/Tf fluorescence ratios of both compartments by a factor such that the mean IgA/Tf ratio of the sorting endosomes equaled one. Data from different cells were then pooled. Images of OG-IgA and TxR-Tf were collected simultaneously, while diD-LDL images were collected separately to prevent bleed-through of the red image to the far-red detector. Unstandardized ratios varied from 0.22 to 2.99, demonstrating that the method has a 14-fold dynamic range sufficient to distinguish potential differences between sorting endosomes and recycling endosomes. It should be stressed that endosome classifications were conducted very conservatively, such that only endosomes clearly labeled with LDL were identified as sorting endosomes and only endosomes clearly lacking LDL in cells with significant LDL uptake were classified as recycling endosomes.

Enzymatic fluorescence quenching

To biochemically evaluate colocalization, we used a biochemical assay in which the presence of HRP-Tf in a compartment containing diI-LDL is demonstrated by the HRP-mediated quenching of fluorescence that occurs in the presence of diaminobenzidine (DAB) and hydrogen peroxide. Cells grown on glass coverslips were incubated for 15 minutes with 10 $\mu\text{g}/\text{ml}$ diI-LDL, 5 $\mu\text{g}/\text{ml}$ OG-Tf and 20 $\mu\text{g}/\text{ml}$ HRP-Tf and fixed. A vertical series of images of the diI-LDL and OG-Tf fluorescence from a field of cells was then collected. The dish was then treated with DAB and hydrogen peroxide (Pierce, Rockford, IL) for 2 minutes and a second vertical series of images of the same field was collected.

Acknowledgments

This work was supported by N.I.H. grant R29DK51098 (K.D.), a fellowship from the American Heart Association, Indiana Affiliate, Inc. (E.W.), the Israel Science Foundation founded by the Israel Academy of Sciences and Humanities – Dorot Science Foundation (B.A.), an American Cancer Society Fellowship PF3666 (S.C.) and N.I.H. grant RO1AI25144 (K.M.).

References

1. von Bonsdorff CH, Fuller SD, Simons K. Apical and basolateral endocytosis in Madin–Darby canine kidney (MDCK) cells grown on nitrocellulose filters. *EMBO J* 1985;4: 2781–2792.

2. Bomsel M, Prydz K, Parton RG, Gruenberg J, Simons K. Endocytosis in filter-grown Madin–Darby canine kidney cells. *J Cell Biol* 1989;109: 3243–3258.
3. Parton RG, Prydz K, Bomsel M, Simons K, Griffiths G. Meeting of the apical and basolateral endocytic pathways of the Madin–Darby canine kidney cell in late endosomes. *J Cell Biol* 1989;109: 3259–3272.
4. Apodaca G, Katz LA, Mostov KE. Receptor-mediated transcytosis of IgA in MDCK cells is via apical recycling endosomes. *J Cell Biol* 1994;125: 67–86.
5. Futter CE, Gibson A, Allchin EH, Maxwell S, Ruddock LJ, Odorizzi G, Domingo D, Trowbridge IS, Hopkins CR. In polarized MDCK cells basolateral vesicles arise from clathrin-gamma-adaptin-coated domains on endosomal tubules. *J Cell Biol* 1998;143: 611–624.
6. Odorizzi G, Pearse A, Domingo D, Trowbridge IS, Hopkins CR. Apical and basolateral endosomes of MDCK cells are interconnected and contain a polarized sorting mechanism. *J Cell Biol* 1996;135: 139–152.
7. Robinson MS. The role of clathrin, adaptors and dynamin in endocytosis. *Curr Opin Cell Biol* 1994;6: 538–544.
8. Johnson LS, Dunn KW, Pytowski B, McGraw TE. Endosome acidification and receptor trafficking: bafilomycin A1 slows receptor externalization by a mechanism involving the receptor's internalization motif. *Mol Biol Cell* 1993;4: 1251–1266.
9. Mayor S, Presley JF, Maxfield FR. Sorting of membrane components from endosomes and subsequent recycling to the cell surface occurs by a bulk flow process. *J Cell Biol* 1993;121: 1257–1269.
10. Dunn KW, McGraw TE, Maxfield FR. Iterative fractionation of recycling receptors from lysosomally destined ligands in an early sorting endosome. *J Cell Biol* 1989;109: 3303–3314.
11. Geuze HJ, Slot JW, Strous GJ, Lodish HF, Schwartz AL. Intracellular site of asialoglycoprotein receptor-ligand uncoupling: double-label immunoelectron microscopy during receptor-mediated endocytosis. *Cell* 1983;32: 277–287.
12. Griffiths G, Back R, Marsh M. A quantitative analysis of the endocytic pathway in baby hamster kidney cells. *J Cell Biol* 1989;109: 2703–2720.
13. Marsh M, Griffiths G, Dean GE, Mellman I, Helenius A. Three-dimensional structure of endosomes in BHK-21 cells. *Proc Natl Acad Sci USA* 1986;83: 2899–2903.
14. Verges M, Havel RJ, Mostov KE. A tubular endosomal fraction from rat liver: Biochemical evidence of receptor sorting by default. *Proc Natl Acad Sci USA* 1999;96: 10146–10151.
15. Sheff DR, Daro EA, Hull M, Mellman I. The receptor recycling pathway contains two distinct populations of early endosomes with different sorting functions. *J Cell Biol* 1999;145: 123–139.
16. Casanova JE, Wang X, Kumar R, Bhartur SG, Navarre J, Woodrum JE, Altschuler Y, Ray GS, Goldenring JR. Association of Rab25 and Rab11a with the apical recycling system of polarized Madin–Darby canine kidney cells. *Molecular Biology of the Cell* 1999;10: 47–61.
17. Goldenring JR, Soroka CJ, Shen KR, Tang LH, Rodriguez W, Vaughan HD, Stoch SA, Modlin IM. Enrichment of rab11, a small GTP-binding protein, in gastric parietal cells. *Am J Physiol* 1994;267: G187–G194.
18. van Ijzendoorn SC, Hoekstra D. The subapical compartment: a novel sorting centre? *Trends Cell Biol* 1999;9: 144–149.
19. Knight A, Hughson E, Hopkins CR, Cutler DF. Membrane protein trafficking through the common apical endosome compartment of polarized Caco-2 cells. *Mol Biol Cell* 1995;6: 597–610.
20. van Ijzendoorn SC, Hoekstra D. Glyco)sphingolipids are sorted in sub-apical compartments in HepG2 cells: a role for non-Golgi-related intracellular sites in the polarized distribution of (glyco)sphingolipids. *J Cell Biol* 1998;142: 683–696.
21. Zacchi P, Stenmark H, Parton RG, Orioli D, Lim F, Giner A, Mellman I, Zerial M, Murphy C. Rab17 regulates membrane trafficking through apical recycling endosomes in polarized epithelial cells. *J Cell Biol* 1998;140: 1039–1053.
22. Ullrich O, Reinsch S, Urbe S, Zerial M, Parton RG. Rab11 regulates recycling through the pericentriolar recycling endosome. *Journal of Cell Biology* 1996;135: 913–924.

23. Barroso M, Sztul ES. Basolateral to apical transcytosis in polarized cells is indirect and involves BFA and trimeric G protein sensitive passage through the apical endosome. *J Cell Biol* 1994;124: 83–100.
24. Geuze HJ, Slot JW, Strous GJ, Peppard J, von Figura K, Hasilik A, Schwartz AL. Intracellular receptor sorting during endocytosis: comparative immunoelectron microscopy of multiple receptors in rat liver. *Cell* 1984;37: 195–204.
25. Gibson A, Futter CE, Maxwell S, allchin EH, Shipman M, Kraehenbuhl JP, Domingo D, Odorizzi G, Trowbridge IS, Hopkins CR. Sorting mechanisms regulating membrane protein traffic in the apical transcytotic pathway of polarized MDCK cells. *J Cell Biol* 1998;143: 81–94.
26. Ren M, Xu G, Zeng J, De Lemos-Chiarandini C, Adesnik M, Sabatini DD. Hydrolysis of GTP on rab11 is required for the direct delivery of transferrin from the pericentriolar recycling compartment to the cell surface but not from sorting endosomes. *Proc Natl Acad Sci USA* 1998;95: 6187–6192.
27. Maxfield FR, Schlessinger J, Shechter Y, Pastan I, Willingham MC. Collection of insulin, EGF and alpha2-macroglobulin in the same patches on the surface of cultured fibroblasts and common internalization. *Cell* 1978;14: 805–810.
28. van Steensel B, van Binnendijk EP, Hornsby CD, van der Voort HT, Krozowski ZS, de Kloet ER, van Driel R. Partial colocalization of glucocorticoid and mineralocorticoid receptors in discrete compartments in nuclei of rat hippocampus neurons. *J Cell Sci* 1996;109: 787–792.
29. Hunziker W, Male P, Mellman I. Differential microtubule requirements for transcytosis in MDCK cells. *EMBO J* 1990;9: 3515–3525.
30. Calhoun BC, Lapierre LA, Chew CS, Goldenring JR. Rab11a redistributes to apical secretory canaliculus during stimulation of gastric parietal cells. *Am J Physiol* 1998;275: C163–C170.
31. Green EG, Ramm E, Riley NM, Spiro DJ, Goldenring JR, Wessling R. Rab11 is associated with transferrin-containing recycling compartments in K562 cells. *Biochem Biophys Res Commun* 1997;239: 612–616.
32. Moore RH, Tuffaha A, Millman EE, Dai W, Hall HS, Dickey BF, Knoll BJ. Agonist-induced sorting of human beta2-adrenergic receptors to lysosomes during downregulation. *J Cell Sci* 1999;112: 329–338.
33. Moyer BD, Loffing J, Schwiebert EM, Loffing-Cueni D, Halpin PA, Karlson KH, Ismailov II, Guggino WB, Langford GM, Stanton BA. Membrane trafficking of the cystic fibrosis gene product, cystic fibrosis transmembrane conductance regulator, tagged with green fluorescent protein in Madin–Darby canine kidney cells. *J Biol Chem* 1998;273: 21759–21768.
34. Vilhardt F, Nielsen M, Sandvig K, van Deurs B. Urokinase-Type Plasminogen Activator Receptor Is Internalized by Different Mechanisms in Polarized and Nonpolarized Madin–Darby Canine Kidney Epithelial Cells. *Mol Biol Cell* 1999;10: 179–195.
35. Hughson EJ, Hopkins CR. Endocytic pathways in polarized Caco-2 cells: identification of an endosomal compartment accessible from both apical and basolateral surfaces. *J Cell Biol* 1990;110: 337–348.
36. Gruenberg J, Maxfield FR. Membrane transport in the endocytic pathway. *Curr Opin Cell Biol* 1995;7: 552–563.
37. Mukherjee S, Ghosh RN, Maxfield FR. Endocytosis. *Physiol Rev* 1997;77: 759–803.
38. Ghosh RN, Gelman DL, Maxfield FR. Quantification of low density lipoprotein and transferrin endocytic sorting HEp2 cells using confocal microscopy. *J Cell Sci* 1994;107: 2177–2189.
39. Hunziker W, Peters PJ. Rab17 localizes to recycling endosomes and regulates receptor-mediated transcytosis in epithelial cells. *J Biol Chem* 1998;273: 15734–15741.
40. Cardone MH, Smith BL, Song W, Mochly-Rosen D, Mostov KE. Phorbol myristate acetate-mediated stimulation of transcytosis and apical recycling in MDCK cells. *J Cell Biol* 1994;124: 717–727.
41. Musch A, Xu H, Shields D, Rodriguez-Boulan E. Transport of vesicular stomatitis virus G protein to the cell surface is signal mediated in polarized and nonpolarized cells. *J Cell Biol* 1996;133: 543–558.
42. Yoshimori T, Keller P, Roth MG, Simons K. Different biosynthetic transport routes to the plasma membrane in BHK and CHO cells. *J Cell Biol* 1996;133: 247–256.
43. Presley JF, Mayor S, Dunn KW, Johnson LS, McGraw TE, Maxfield FR. The End2 mutation in CHO cells slows the exit of transferrin receptors from the recycling compartment but bulk membrane recycling is unaffected. *J Cell Biol* 1993;122: 1231–1241.
44. Jing SQ, Spencer T, Miller K, Hopkins C, Trowbridge IS. Role of the human transferrin receptor cytoplasmic domain in endocytosis: localization of a specific signal sequence for internalization. *J Cell Biol* 1990;110: 283–294.
45. Brewer CB. Cytomegalovirus plasmid vectors for permanent lines of polarized epithelial cells. *Methods Cell Biol* 1994;43 Pt A: 233–245.
46. Breitfeld PP, Casanova JE, Harris JM, Simister NE, Mostov KE. Expression and analysis of the polymeric immunoglobulin receptor in Madin–Darby canine kidney cells using retroviral vectors. *Methods Cell Biol* 1989;32: 329–337.
47. White S, Miller K, Hopkins C, Trowbridge IS. Monoclonal antibodies against defined epitopes of the human transferrin receptor cytoplasmic tail. *Biochim Biophys Acta* 1992;1136: 28–34.
48. Barth AI, Pollack AL, Altschuler Y, Mostov KE, Nelson WJ. NH₂-terminal deletion of beta-catenin results in stable colocalization of mutant beta-catenin with adenomatous polyposis coli protein and altered MDCK cell adhesion. *J Cell Biol* 1997;136: 693–706.
49. Yamashiro DJ, Tycko B, Fluss SR, Maxfield FR. Segregation of transferrin to a mildly acidic (pH 6.5) para-Golgi compartment in the recycling pathway. *Cell* 1984;37: 789–800.
50. Pitas RE, Innerarity TL, Weinstein JN, Mahley RW. Acetoacetylated lipoproteins used to distinguish fibroblasts from macrophages in vitro by fluorescence microscopy. *Arteriosclerosis* 1981;1: 177–185.
51. Maxfield FR, Dunn KW. In Herman B, Jacobsen K (Eds.), *Studies of Endocytosis Using Image Intensification Fluorescence Microscopy and Digital Image Analysis*. New York: Alan R. Liss, 1990: 357–371.
52. Dunn KW, Mayor S, Myers JN, Maxfield FR. Applications of ratio fluorescence microscopy in the study of cell physiology. *FASEB J* 1994;8: 573–582.
53. Dunn KW, Maxfield FR. Ratio imaging instrumentation. *Methods Cell Biol* 1998;56: 217–236.